Si/Al ratio and its impact on CO_2 adsorption in TiO_2-Zeolite

K.M. Álvarez-Gómez, M. de los A. Velasco-Hernández, E. Ayala-Herrera, M.D. Guevara-Espinosa, R. Portillo Reyes

The aim of this study was to analyze the Si/Al ratio in titanium dioxide (TiO_2) and Zeolite composites (Erionite, Clinoptilolite and Mordenite) and its influence on carbon dioxide (CO_2) adsorption, seeking to optimize materials for greenhouse gas capture. Composites were synthesized by the sol-gel method, varying the proportions of TiO_2 and zeolites (25-75 and 75-25) as a function of weight. They were characterized using techniques such as Energy Efficiency Spectroscopy (EDS) to determine the Si/Al ratio, X-ray diffraction for crystal size, and N_2 adsorption for surface area. The results showed that, in most of the composites, the Si/Al ratio decreases compared to the original zeolites, except in those based on Mordenite, which maintain high values due to their greater chemical stability. The decrease in the Si/Al ratio was correlated with an increase in the CO_2 affinity, especially in the TiO_2-Erionite composites, which presented the lowest Si/Al values (3.29) and higher adsorption capacity. In contrast, composites with Mordenite exhibited a lower CO_2 affinity, but a higher surface area (456 m^2/g). In conclusion, the Si/Al ratio is a key parameter to optimize CO_2 adsorption, and the intrinsic properties of each zeolite significantly affect the composite performance. These materials have potential for applications in environmental mitigation technologies.

Introduction

Currently, a major problem is climate change caused by global warming caused by greenhouse gas (GHG) emissions that have caused serious harm to humans, such as accelerating the melting of glaciers, raising sea levels, causing forest fires, etc. In this context, the reduction of emissions and the capture of GHGs have become a global concern, and research to reduce their concentration in the atmosphere is a task that cannot be postponed [1-2]. Among the most important greenhouse gases we can find methane (CH_4), nitrous oxide (N_2O) and carbon dioxide (CO_2). These gases are capable of trapping solar radiation and increasing global warming [3]. The Environmental Protection Agency (EPA) indicates that the most emitted GHGs are nitrogen dioxide (NO_2) at 0.08%, CH_4 at 2.25%, and CO_2 at 97.37% [4]. It is worth noting that CO_2 constitutes a component of the atmosphere, accounting for between 0.03% and 0.04%. However, due to continued industrial development and fossil fuel consumption, atmospheric CO_2 continues to increase, causing a growing greenhouse effect [5].

The seriousness of climate change and global warming has been internationally recognized. Therefore, several countries have initiated various strategies and/or plans to counteract the damage caused. Since 1880, the Earth has been warming at an accelerated rate, reaching 1.1°C today. Compared to the pre-industrial era, atmospheric CO_2 concentrations have increased by 40% (reached in the summer of 2023). The Intergovernmental Panel on Climate Change (IPCC) reports that CO_2 emissions must be reduced by at least 45% by 2030 compared to 2010 levels and reach net-zero carbon emissions by 2050 to limit the global average. Some articles predict that if GHG emissions continue to increase, the year 2035 may become the point of no return [6-7]. This raises the need to reduce and control CO_2 emissions or to find ways to reduce them and implement energy more efficiently [8]. Among the various environmental solutions proposed for CO_2 emissions is the research into effective techniques for CO_2 conversion [9], such as plasma-chemical [10], photochemical [11], biochemical [12], solar-bioelectrochemical [1], thermochemical [13], and photocatalytic [14].

Photocatalysis is a method based on solar irradiation, which makes it low-cost, and has thus been considered a sustainable energy source for promoting CO_2 conversion [15]. Currently, CCUS technology is based on photocatalytic conversion, which is a promising new approach to effectively reduce CO_2 emissions and concentrations in ambient air [16].

The appropriate characteristics for selecting a good photocatalyst are: (i) the ability to absorb radiation from a broad spectral range; (ii) the appropriate position of the semiconductor energy bands relative to the redox reaction potentials; (iii) high mobility and long diffusion path of charge carriers; (iv) thermodynamic, electrochemical, and photoelectrochemical stability [17]. These characteristics can be provided by semiconductor oxides such as tungsten oxide (WO_3), zinc oxide (ZnO), and titanium dioxide (TiO_2) [18]. TiO_2 is the most prominent photocatalyst due to its high chemical and biological stability, nontoxicity, low cost, corrosion resistance, and availability compared to other materials [19-20].

This semiconductor oxide (TiO_2) has three phases: brookite, rutile, and anatase. Brookite TiO_2 has an orthorhombic crystal structure and is not well known. Meanwhile, rutile TiO_2 has a tetragonal prismatic crystal

K. M. Álvarez-Gómez ✉, M. de los A. Velasco-Hernández
Departamento de Investigación en Zeolitas – ICUAP, Benemérita Universidad Autónoma de Puebla, Puebla, Pue., 72570, México.

E. Ayala-Herrera, M. D. Guevara-Espinosa
Facultad de Ingeniería Química, Benemérita Universidad Autónoma de Puebla, Puebla, Pue., 72570, México.

R. Portillo Reyes
Facultad de Ciencias Químicas Benemérita Universidad Autónoma de Puebla, Puebla, Pue., 72570, México.

Received: September 10th, 2025.
Accepted: November 6th, 2025.
Published: December 22nd, 2025.

https://doi.org/10.47566/2025_syv38_1-251201

structure and is usually used as a pigment in paint. Anatase TiO_2 has a tetragonal bipyramidal crystal structure and is used as a photocatalyst under UV irradiation [21]. However, semiconductor oxides do not have a large surface area, so it is necessary to increase their surface area with the help of support materials such as zeolites [22]. It is worth mentioning that zeolites are hydrated aluminosilicate materials that have a three-dimensional porous structure which have cations of alkaline earth elements (magnesium, calcium and infrequently barium and strontium), alkaline elements (sodium, potassium) or other monovalent or multivalent metals. They contain channels and free space, which are characteristics of porous materials, which generates a very large surface area [23]. By combining these properties of both TiO_2 and Zeolites, the adsorption potential of contaminants composed of TiO_2-Zeolite can be improved [24]. There are several studies on the use of zeolite photocatalysts for CO_2 reduction [25], as well as specific studies on TiO_2-Zeolite for CO_2 removal by UV lamp irradiation [26-29].

This work aims to study CO_2 adsorption in mixtures of TiO_2 with three porous zeolites (erionite, mordenite, and clinoptilolite), in ratios of 25:75 and 75:25 (TiO_2-Zeolite). The aim is to analyze the influence of zeolite on adsorption, considering its surface area and intrinsic properties. For this purpose, gas chromatography and adsorption isotherm models (Langmuir, Dubinin and Freundlich) are used to evaluate the adsorption process in photocatalysts, as a key step before a possible CO_2 conversion.

Material and methods

Materials

Titanium isopropoxide (Sigma-Aldrich, CAS No. 546-68-9), isopropanol (J. T. Baker, CAS No. 67-63-00), ammonium hydroxide (EM SCIENCE, CAS No. 1336-21-6), and natural zeolite Erionite (by its ERI code corresponding to the International Zeolite Association (IZA), obtained from the deposits of Agua Prieta, Sonora), Clinoptilolite (by its HEU code corresponding to the IZA, obtained from the deposits of San Gabriel Chilac, Puebla), and Mordenite (by its MOR code corresponding to the IZA, obtained from the deposits of Magdalena, Oaxaca). Table I presents the nomenclature used for TiO_2-Zeolite composites.

Table I. Nomenclature used in TiO_2-Zeolite composites.

Sample	Content in weight%	IZA Code	Deposit
TiO_2	100% titanium dioxide	N/A	N/A
TE25	25% titanium dioxide 75 % erionite	ERI	Agua Prieta, Sonora
TE75	75% titanium dioxide 25 % erionite	ERI	Agua Prieta, Sonora
TC25	25% titanium dioxide 75 % clinoptilolite	HEU	San Gabriel Chilac, Puebla
TC75	75% titanium dioxide 25 % clinoptilolite	HEU	San Gabriel Chilac, Puebla
TM25	25% titanium dioxide 75 % mordenite	MOR	Magdalena, Oaxaca
TM75	75% titanium dioxide 25 % mordenite	MOR	Magdalena, Oaxaca

N/A: Not applicable

Methods

The sol-gel method was used to obtain the TiO_2 nanoparticles, which consisted of the following steps (see Figure 1):

i. Mixing: The precursors were mixed using a griddle with constant stirring (titanium isopropoxide with isopropanol) for approximately 30 min.
ii. Gelation: Ammonium hydroxide was added to generate gelation.
iii. Aging: The particles were allowed to settle for approximately 24 hours.
iv. Drying: Drying was carried out at 80 °C for approximately 6 hours to remove organic solvents.
v. Sintering: The TiO_2 nanoparticle networks were restructured at 500°C for approximately 1 hour.

In the case of the composites, zeolite was added in situ after gelation. The materials obtained were: TiO_2: contains 100% titanium dioxide, TE25: contains 25% titanium dioxide and 75% Erionite, TE75: contains 75% titanium dioxide and 25% Erionite, TC25: contains 25% titanium dioxide and 75% Clinoptilolite, TC75: contains 75% titanium dioxide and 25% Clinoptilolite, TM 25: contains 25% titanium dioxide and 75% Mordenite, TM75: contains 75% titanium dioxide and 25% Mordenite. These percentage ratios are based on the weight percentage.

Determination of the Si/Al ratio

The Si/Al atomic ratio is generally determined through elemental chemical analysis of zeolite samples, a non-destructive, generally slow, and laborious procedure. EDS microanalysis is performed by measuring the energy and intensity distribution of X-rays generated by the action of the primary electron beam on the sample, using an energy-dispersive detector [30]. The Si/Al ratio is estimated to be using EDS. The sample is placed in the equipment and different areas on the surface of the material to be studied are measured (to obtain a true value). This results in the weight percentages of the elements contained in each area of the sample, and an estimated average is obtained. The semi-quantitative values obtained allow establishing a Si/Al relationship [31-33].

Figure 1. Sol-Gel process.

Structural and physicochemical parameters

The average crystal size was determined using the Scherrer equation (also known as the Debye-Scherrer equation for estimating crystallite size). This equation considers the diffraction peak width of the material (powder) with the average volume dimensions of the crystallites in a polycrystalline material [34].

$$\beta_s(2\theta)_{hkl} = \frac{K\lambda}{FWHM\cos\theta_{hkl}} \quad (1)$$

Where, β_s is the crystal size is, which is a function of the peak width, K is a dimensionless factor representing the particle shape in the Debye-Scherrer equation. Its value is usually close to unity, ranging from 0.8 to 1.39, λ is the wavelength of the X-ray radiation used, FWHM (Full Width at Half Maximum) is the full width at half maximum of a peak. When implementing the Scherrer equation, it is considered that the crystallite size and the size of the polycrystalline aggregate are not the same. It is worth mentioning that a crystallite is a discrete diffractive domain that is consistently scattering X-rays.

To determine surface areas, the Quantachrome Autosorb-1C nitrogen adsorption system was used, using nitrogen as the carrier gas at a temperature of 77 K. Measurements were made over a relative pressure (P/P_0) range from 0.01 to 0.99. This technique is the most used for surface area characterization.

CO_2 adsorption experiments on substrates were performed on a Varian CX3900 gas chromatograph with a thermal conductivity detector. The chromatographic columns were made of stainless steel (with an internal diameter of 5 mm and a length of 50 cm) and packed with TiO_2 or TiO_2-Zeolite granules equivalent to 0.250 mm mesh size. To carry out CO_2 adsorption, the samples were pretreated with helium (He) loading at a temperature of 300 °C. Subsequently, CO_2 injections were performed in a column in order to obtain the retention time. The gas adsorption isotherms on the zeolites were measured at various temperatures (220, 240, 260, 280 and 300 °C); The adsorbed amount was assessed as a function of pressure using the chromatographic peak maximum method (GC peak maximum method) using helium (30 cm^3/min) as the carrier gas. Experimentally determined data on adsorption isotherms helped determine isostatic heats using the Clausius-Clapeyron equation at low coverage levels.

Data corresponding to CO_2 adsorption on TiO_2 and TiO_2-Zeolite samples were fitted to standard Freundlich isothermal models using linear regression to determine the adsorption parameters relevant to each of the above approaches.

The Freundlich adsorption equation can be written as [35]:

$$a = K_F + p^{1/n} \quad (2)$$

Where a is the amount of adsorbed substance per unit mass of the adsorbent, K_F is the Freundlich adsorption constant indicating the adsorption capacity of the adsorbent, p is the gas pressure and n is an exponential factor representing the adsorption intensity. Linear regression fits the CO_2 adsorption data to the Langmuir equation. It is also possible to determine the Henry constant (K_H) at different temperatures for the series of adsorbent-adsorption pairs, from the gas adsorption data at low variations using the following expression [36]:

$$K_H = \lim_{p\to 0}(a/a_m p) \quad (3)$$

Where a represents the amount adsorbed on the solid walls at pressure p, while am is the capacity of the monolayer evaluated from the Langmuir equation [37]:

$$\theta = a/a_m = K_p/(1+K_p) \quad (4)$$

Where θ corresponds to the surface coverage fraction, a is the volume of gas adsorbed by the solid, am is the volume of monolayer gas molecules covering the entire surface of the solid and completely occupied by the adsorbent, K_p is the Langmuir constant at partial pressure of the adsorbent.

$$1/a = 1/a_m + 1/a_m K_p \quad (5)$$

The standard adsorption energies (−ΔUo) can be found from the temperature dependence of the Henry constants K_H (at low pressures $K_H \approx K_F$), a relationship that is consistent with the traditional Van´t Hoff form [38]:

$$(\partial \ln K_H/\partial T) = \Delta U_o/RT^2\,;\; K_H = K_o \exp(-\Delta U_o/RT) \quad (6)$$

Where $\Delta U_o = \Delta H_o + RT$; ΔH_o is the standard adsorption enthalpy, R is the universal gas constant, and K_o is the Van't Hoff pre-exponential factor.

The isosteric heat of adsorption, q_{st} (kcal/mol), at different adsorbate loadings can be evaluated from the adsorption isotherm data using a Clausius-Clapeyron equation:

$$[\partial \ln p/\partial T]_a = q_{st}\; a/RT^2. \quad (7).$$

Results and discussion

Physical-chemical studies of materials

Table II shows the Si/Al ratio obtained from the EDS analysis. The sample with the highest Si/Al ratio is the TM25 sample with a value of 8.48, while the lowest value was 3.29 for the TE25 sample. The order of the Si/Al ratio in decreasing order is as follows TM25 > TM75 > MOR > CLI > ERI > TC25 > TC75 > TE75 > TE25 with the corresponding values 8.48 > 7.56 > 5.32 > 5.22 > 4.69 > 4.23 > 4.05 > 4.01 > 3.29. It is important to note that increasing the Si/Al ratio indicates that it has a greater amount of silica (Si), it is worth mentioning that silica is a hydrophobic material and therefore does not have the capacity to absorb water. The affinity for CO_2 increases with a decrease in the Si/Al ratios [28]. Based on the above, it is observed that the composite material with the highest adsorption capacity, according to the Si/Al ratio, is TE25. This is because its lower Si/Al ratio increases its adsorption capacity, which also improves its ability to adsorb CO_2. However, its catalytic lifetime is limited due to the low Si/Al ratio [28]. In contrast, the TM25 sample has a Si/Al ratio of 8.48.

This study shows that, as the amount of zeolite (erionite, clinoptilolite, and mordenite) increases, so does the Si/Al ratio. This implies a possible increase in the adsorption capacity of compounds with higher amounts of zeolite. The overall decrease observed in the Si/Al ratio in the composites, compared to the starting zeolites, can be

Table II. Physicochemical properties of the materials.

Sample	Si/Al	Average crystallite size (nm)	A_B (m^2/g)	C_B	A_L (m^2/g)	K_L	A_{ext} (m^2/g)	W_o (cc/g)	ΣW (cc/g)
TiO_2	-----	12.66	34.5	222.0	54.1	24.4	30.9	0.0016	0.7768
ERI	4.69	----------	188.3	-295.2	241.6	587.7	16.6	0.0763	0.1013
TE25	3.29	22.25	204.1	-49.4	300.4	109.7	50.8	0.0785	0.0168
TE75	4.01	9.72	301.7	-600.7	301.7	-600.7	195.3	0.0534	0.0390
CLI	5.22	--------	16.0	235.8	26.9	16.6	14.3	0.0007	0.0343
TC25	4.23	26.23	57.7	68.7	96.9	14.1	57.7	0.0000	0.1121
TC75	4.05	30.71	70.6	92.8	102.2	26.5	70.6	0.0000	0.1437
MOR	5.32	-----	288.6	-84.0	405.0	335.5	41.9	0.1213	0.1854
TM25	8.48	51.12	327.5	-85.6	456.0	190.4	74.4	0.1230	0.0269
TM75	7.56	22.11	159.9	-188.3	225.1	68.2	69.9	0.0419	0.1792

A_B, BET surface area; C_B, BET constant; A_L, Langmuir surface area; K_L, Langmuir constant;
A_{ext}, External surface area; W_o, micropore volume; ΣW, Total volume.

attributed to the incorporation of TiO_2 during the sol-gel process. This method can cause slight leaching of aluminum into the zeolitic matrix or its chemical interaction with the TiO_2, altering the Si/Al ratio. In the case of the TiO_2-MORN composites, the Si/Al ratio remained high, possibly due to the greater chemical stability of mordenite during the synthesis process, which minimized aluminum loss or structural alteration.

The affinity of the composites for CO_2 is closely linked to their Si/Al ratio. Studies have shown that a lower Si/Al ratio indicates a higher aluminum content, which increases the density of exchangeable cations in the zeolitic structure. These cations act as active sites for CO_2 adsorption, improving the gas capture capacity [39].

The initial composition of the zeolite influences the Si/Al ratio of the resulting composites. Zeolites with lower Si/Al ratios, such as erionite, have a higher cation density, which can favor CO_2 adsorption. On the other hand, zeolites with higher Si/Al ratios, such as mordenite, exhibit different adsorption capacities due to their lower cation density. These structural and compositional differences directly affect the adsorptive properties of TiO_2-Zeolite composites [40]. In the case of clinoptilolite, its moderate Si/Al ratio suggests that its CO_2 adsorption capacity would be lower than that of zeolites with lower Si/Al ratios, such as erionite, but higher than those with higher ratios, such as some forms of mordenite. This correlation is due to the fact that a higher proportion of aluminum in the zeolitic structure increases the negative charge density, which in turn increases the attraction of CO_2 molecules to the compensating cations present at the adsorption sites [40].

Regarding the average crystal size (obtained from X-ray diffraction patterns using the Scherrer equation), it can be observed that the increase becomes considerable with increasing amounts of zeolites in the samples, except for the TC25 sample, which maintains the same average crystal size. This is perhaps due to the Si/Al ratio, which does not change drastically.

Regarding the surface areas obtained by nitrogen adsorption, the TM25 sample shows a larger surface area, with a value of 456.0 m^2/g. This result is linked to its Si/Al ratio of 8.48, which indicates a higher adsorption capacity. Furthermore, this is considerably higher and favors the adsorption process.

CO_2 adsorption isotherms

The dynamic chromatographic method was used to evaluate the adsorption isotherms from the injection pulse data derived from the elution curves of the adsorbents in the composite study.

Figure 2 shows the CO_2 adsorption isotherms on TiO_2 nanoparticles, where a nearly linear behavior with a small favorable curvature can be observed, while Figure 3 shows the CO_2 adsorption isotherms on the TiO_2-Zeolite composites.

In the case of the samples containing TiO_2 and erionite (Figures 3a and 3b), the incorporation of erionite zeolite generates isotherms with a more concave curvature compared to the isotherms of pure TiO_2. This indicates a

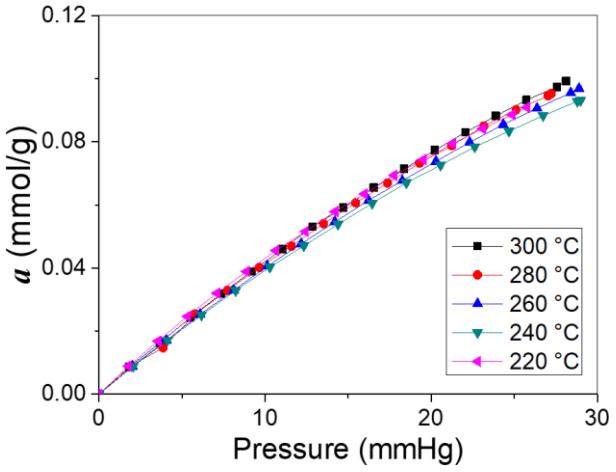

Figure 2. CO_2 adsorption isotherm on TiO_2 nanoparticles.

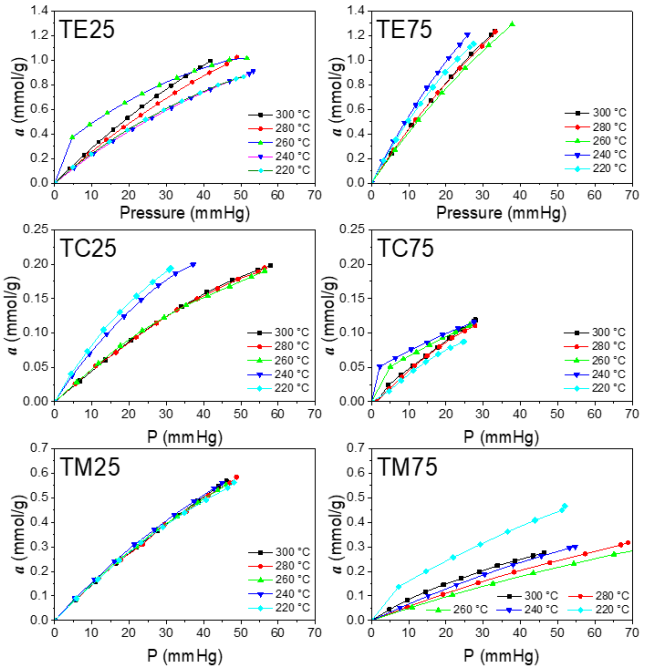

Figure 3. CO_2 adsorption isotherms on TiO_2-Zeolite composites.

lower adsorption capacity in the TE25 sample and a higher adsorption capacity in the sample with the lower erionite content (TE75). This behavior is related to the Si/Al ratio, where it is evident that TE25 exhibits less favorable values for adsorption.

In the case of the samples containing TiO_2 and erionite (TE25 and TE75), the incorporation of erionite zeolite generates isotherms with a more concave curvature compared to the isotherms of pure TiO_2. This indicates a lower adsorption capacity in sample TE25 and a higher capacity in the sample with lower erionite content (TE75). This behavior is related to the Si/Al ratio, where it is evident that TE25 exhibits less favorable values for adsorption.

The TiO_2-CLI samples (corresponding to TC25 and TC75) exhibit more pronounced concave curvatures than the TiO_2-Erionite compounds. It is also evident that the addition of a greater amount of clinoptilolite increases the adsorption capacity of the sample.

The TiO_2-Mordenite compounds, although not as concave as the TiO_2-Clinoptilolite samples, exhibit the same behavior: a higher zeolite content results in greater adsorption capacity.

Table III shows the adsorption constants of adsorbed CO_2 at 25 mmHg for the different materials evaluated. Pure TiO_2, at 220 °C, has an adsorption constant of 0.0893 mmol/g. However, with the addition of the TE75 composition at 220 °C, the adsorption constant increases significantly to 1.0682 mmol/g. This increase is attributed to the addition of a porous material to the TiO_2, which enhances its adsorption capacity. It is worth noting that the highest adsorption constants, at both 220 °C and 300 °C, were recorded in the TE75 and TE25 samples, which had the lowest Si/Al ratios, with values of 4.01 and 3.29, respectively. This demonstrates that the affinity for CO_2 increases as the Si/Al ratio in the compounds decreases.

Study of the constants of Henry, Langmuir, and Freundlich

Table III presents the Henry, Langmuir, and Freundlich constants. It is worth mentioning that for low pressures $K_H \approx K_F$, the theoretical Langmuir equation was developed assuming the following [41]:

(1) There is a fixed number of accessible sites available on the adsorbent surface, and all sites have the same energy (the homogeneous surface).
(2) Adsorption is irreversible.
(3) Once an adsorbate occupies a site, no further adsorption can occur at that site.
(4) There is no longer interaction between the adsorbed species. All of these points indicate that a monolayer has been generated.

In accordance with the above, we can observe in Table IV where the R_L (Langmuir correlation constant) values fit the Langmuir equation (This is evidenced by analyzing the Langmuir and Freundlich constants. Positive constants indicate a good fit to these models, while the correlation coefficient confirms the accuracy of the fit with respect to the experimental values) indicating that a monolayer is produced on the surface. While negative values indicate a deviation from the ideal behavior of the model or a limitation in the mathematical fit due to experimental noise or dispersion of the points, the pressure or temperature range does not fit well to the ideal model (monolayer or linear equilibrium) or the observed phenomenon does not strictly follow the theoretical isotherm. It is also shown that the adsorption phenomenon is governed by an isothermal process because the a_m and K_L values decreased with increasing temperature [41]. In the case of the Freundlich isotherm model, it is the first known empirical equation that can be applied to non-ideal adsorption on heterogeneous surfaces, as well as to multilayer adsorption (i.e., several adsorbate layers can bind to the adsorbent) [41]. The Freundlich correlation constant (R_F) values do not fit as perfectly as those of Langmuir, indicating that the predominant adsorption process is a monolayer process. The Freundlich constant (K_F) or Freundlich coefficient represents a deviation from linearity of adsorption.

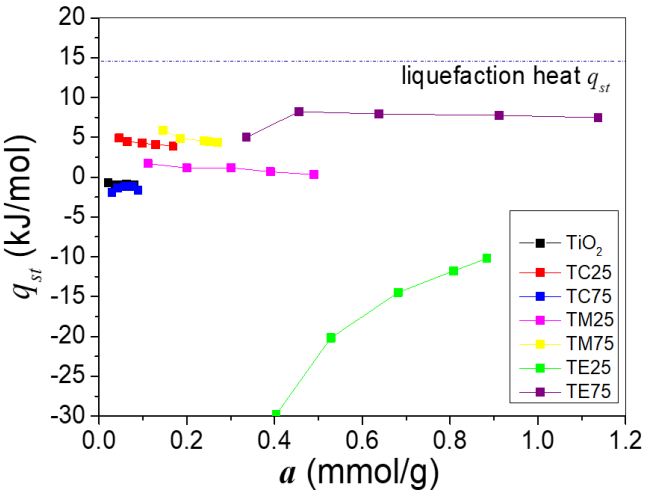

Figure 4. Isosteric heat of CO_2 in the different composites.

Table III. Comparison of the adsorption constants in the different composites at temperatures of 220 ºC and 300 ºC at a pressure of 25 mmHg.

	Adsorption constants (a) (*mmol/g*)							
	TiO_2		TiO_2-ERI		TiO_2-CLI		TiO_2-MOR	
Weight%	220 °C	300 °C	220 °C	300 °C	220 °C	300 °C	220 °C	300 °C
(75-25)	*****	*****	1.0682	0.9978	0.0880	0.1068	0.2809	0.1760
(25-75)	*****	*****	0.5294	0.6526	0.1690	0.1061	0.3371	0.3351
(100)	0.0893	0.0916	*****	*****	*****	*****	*****	*****

Table IV. Henry, Freundlich, and Langmuir parameters for CO_2 adsorption on TiO_2-Zeolite composites.

Sample	**T** (*°C*)	$\mathbf{K_H \approx K_L}$ (*mmol/g·mmHg*)	$\mathbf{a_m}$ (*mmol/g*)	$\mathbf{R_L}$	$\mathbf{K_F}$ (*mmol/g·mmHg*)	**N**	$\mathbf{R_F}$
TiO_2	220	-3.675	-52.826	0.999	0.005	1.155	0.998
	240	-2.827	-80.192	0.999	0.004	1.128	0.997
	260	-2.619	-85.397	0.999	0.004	1.115	0.998
	280	-2.677	-81.366	0.990	0.004	1.099	0.995
	300	-2.839	-73.206	0.999	0.005	1.119	0.998
TE25	220	-0.445	-81.300	0.999	0.036	1.223	0.996
	240	-0.345	-116.550	0.999	0.037	1.179	0.997
	260	-0.889	-10.837	0.933	0.182	2.269	0.996
	280	-0.204	-181.488	0.999	0.031	1.112	0.998
	300	-0.223	-145.772	1.000	0.035	1.109	0.998
TE75	220	-0.232	-74.460	0.999	0.068	1.161	0.996
	240	-0.209	-77.101	0.999	0.069	1.128	0.998
	260	-0.186	-119.189	1.000	0.054	1.140	0.998
	280	-0.192	-107.991	0.999	0.057	1.140	0.999
	300	-0.163	-129.870	0.999	0.055	1.119	0.998
TC25	220	-1.916	-59.347	0.999	0.009	1.489	0.998
	240	-1.637	-118.343	0.999	0.011	1.239	0.996
	260	-1.504	-132.625	0.999	0.007	1.210	0.992
	280	-0.989	-217.864	0.998	0.006	1.172	0.995
	300	-1.999	-49.726	0.999	0.006	1.144	0.993
TC75	220	2.966	104.058	0.984	0.003	0.982	0.984
	240	-8.940	-3.178	0.820	0.007	3.062	0.960
	260	-6.950	-10.096	0.943	0.022	2.076	0.990
	280	-1.177	211.864	0.993	0.008	1.280	0.995
	300	-2.302	-78.247	0.998	0.006	1.137	0.999
TM25	220	-0.501	-124.069	0.999	0.020	1.155	0.997
	240	-0.564	-100.908	0.999	0.021	1.162	0.999
	260	-0.476	-128.865	0.999	0.020	1.146	0.998
	280	-0.435	-146.198	0.999	0.019	1.130	0.925
	300	-0.388	-166.112	0.998	0.180	1.105	0.999
TM75	220	-1.537	-29.079	0.971	0.038	1.602	0.996
	240	-0.716	-197.238	0.999	0.029	1.212	0.931
	260	-1.749	-257.731	0.999	0.006	1.136	0.998
	280	-0.745	-223.214	0.999	0.007	1.137	0.931
	300	-1.548	-64.977	0.999	0.013	1.255	0.930

There is a direct relationship between the K_F parameter and the adsorption capacity, since an increase in K_F indicates an increase in adsorption capacity [42]. Table IV shows that the composites have the following order based on K_F: TE75 > TE25 > TM75 > TC75 > TM25 > TC25 > TiO_2. This shows that the composites with the highest adsorption capacity are those with the lowest Si/Al ratio, as is the case of TE75 and TE25, which have a value of 4.01 and 3.29.

Isosteric Heat

The isosteric heat values obtained indicate that adsorption is predominantly physical, with curves that do not exceed the heat of liquefaction of CO_2 (Figure 4). Compared to other studies, these values are consistent with modified zeolitic materials that present efficient physical adsorption but are limited by long-term structural stability. TiO_2-Zeolite composites show isosteric heating similar to those reported for natural zeolites and MOFs (Metal-Organic Materials), such as ZIF-8 deposited on TiO_2 nanotubes, which also combine high surface area with selective adsorption. However, the materials studied here have the advantage of being less expensive and more accessible for commercial applications [43].

Conclusions

TiO_2-Zeolite composites show great potential for CO_2 capture, highlighting that the decrease in Si/Al ratio significantly improves the adsorption capacity due to the increase in exchangeable cation density, as observed in TE75 and TE25, with values of 4.01 and 3.29, respectively. Furthermore, the increase in surface area, as in TM25 with 456 m^2/g, reinforces the adsorption efficiency. The Langmuir model best fits the experimental data evidencing monolayer adsorption, while isosteric analysis confirmed that the interaction is predominantly physical. These results underline the synergy between TiO_2 and zeolites, offering viable and efficient materials for environmental mitigation applications.

Acknowledgements

Authors want to thank the Departamento de Investigación en Zeolitas, ICUAP, and the vice-Rectorate for Research and Graduate studies, from Benemérita Universidad Autónoma de Puebla, for the facilities provided on the execution of this research.

References

[1]. P.C. Sahoo, D. Pant, M. Kumar, R.P. Gupta, U. Srivastava, *Curr. Opin. Electrochem.* **45**, 101513 (2024).
[2]. Z. Wang, M. Wang, X. Hu, *Sens. Actuators A* **370**, 115222 (2024).
[3]. S. Sadra, G. Mohammadi, F. Mondani, *J. Agric. Food Res.* **18**, 101256 (2024).
[4]. Y. Yan, Y.X. Pang, X. Luo, Q. Lin, C.H. Pang, H. Zhang, X. Gao, T. Wu, *Process Saf. Environ. Prot.* **188**, 406 (2024).
[5]. Z. Wang, M. Wang, X. Hu, P. Jia, *Colloids Surf. A* **689**, 133621 (2024).
[6]. S. Cho, Y.S. Jeong, J. H. Huh, *Energy Sustain. Dev.* **80**, 101447 (2024).
[7]. T. Pavel, S. Polina, N. Liubov, *Energy Convers. Manag.* **314**, 118671 (2024).
[8]. S. Li, Z. Tong, M. Haroon, *Transp. Res. D* **133**, 104276 (2024).
[9]. M.U. Rao, D. Vidyasagar, H.S. Rangappa, C. Subrahmanyam, *Catal. Today* **441**, 114887 (2024).
[10]. A.N. Andreev, V.V. Zakharov, V.N. Ochkin, S.Y. Savinov, *Spectrochim. Acta A* **60**, 3361 (2004).
[11]. X. Meng, R. Li, J. Yang, S. Xu, C. Zhang, K. You, B. Ma, H. Guan, Y. Ding, *Chin. J. Catal.* **49**, 2414 (2022).
[12]. Y. Chen, C. Xu, S. Vaidyanathan, *Appl. Energy* **261**, 114420 (2020).
[13]. B. Jiang, Z. Song, B.G. Lougou, H. Zhang, W. Wang, B. Geng, L. Wu, T. Yan, D. Ma, S. Zhang, Y. Shuai, D.S. Takou, *Renew. Energy* **230**, 120818 (2024).
[14]. Z. Xie, W. Zhang, W. Yang, G. Xie, *J. Environ. Chem. Eng.* **12**, 113359 (2024).
[15]. X. Wei, X. Zhang, L. Jin, X. Yang, W. Zou, B. Gao, L. Dong, *Appl. Catal. B* **351**, 123957 (2024).
[16]. G. Yergaziyeva, Z. Kuspanov, M. Mambetova, N. Khudaibergenov, N. Makayeva, C. Daulbayev, *J. CO_2 Util.* **80**, 102682 (2024).
[17]. A. Feliczak-Guzik, *Materials* **16**, 193 (2023).
[18]. A. Ramchiary, Metal-oxide semiconductor photocatalysts for the degradation of organic contaminants. In: *Handbook of Smart Photocatalytic Materials*, Eds. C.M. Hussain, A.K. Mishra (Elsevier, 2020) pp. 23-38.
[19]. X. Wu, Applications of titanium dioxide materials. In: *Titanium Dioxide - Advances and Applications*, Ed. H.M. Ali (IntechOpen, 2021).
[20]. S.J. Armaković, M.M. Savanović, S. Armaković, *Catalysts* **13**, 26 (2023).
[21]. P. Gupta, V. Rathore, *Mater. Today Proc.* **42**, 1345 (2021).
[22]. L.K. Munguti, F.B. Dejene, D.K. Muthee, *Mater. Sci. Eng. B* **289**, 116281 (2023).
[23]. N. Kordala, M. Wyszkowski, *Molecules* **29**, 1069 (2024).
[24]. O. Sacco, V. Vaiano, *Visible light active structured photocatalysts for the removal of emerging contaminants* (Elsevier, 2020).
[25]. A.-Y. Lo, F. Taghipour, *Appl. Mater. Today* **23**, 101042 (2021).
[26]. M. Anpo, H. Yamashita, K. Ikeue, Y. Fujii, S.G. Zhang, Y. Ichihashi, D.R. Park, Y. Suzuki, K. Koyano, T. Tatsumi, *Catal. Today* **44**, 327 (1998).
[27]. K. Ikeue, H. Yamashita, T. Takewaki, M.E. Davis, M. Anpo, *J. Synchrotron Radiat.* **8**, 602 (2001).
[28]. W. Jia, T. Liu, Q. Li, J. Yang, *Catal. Today* **335**, 221 (2019).
[29]. Y. Sun, G. Li, Y. Gong, Z. Sun, H. Yao, X. Zhou, *J. Hazard. Mater.* **124**, 019 (2020).
[30]. J. Li, M. Gao, W. Yan, J. Yu, *Chem. Sci.* **14**, 1935 (2023).
[31]. M. Moshoeshoe, *Am. J. Mater. Sci.* **7**, 196 (2017).
[32]. C.J. Heard, L. Grajciar, P. Nachtigall, *Chem. Sci.* **10**, 5705 (2019).
[33]. D.A. Kennedy, F.H. Tezel, *Microporous Mesoporous Mater.* **262**, 235 (2018).
[34]. M. Basak, Md.L. Rahman, Md.F. Ahmed, B. Biswas, N. Sharmin, *J. Alloys Compd.* **895**, 162694 (2022).
[35]. S. Debnath, R. Das, *Ceram. Int.* **49**, 16199 (2023).
[36]. D.W. Siderius, H.W. Hatch, V.K. Shen, *J. Phys. Chem. B* **126**, 7999 (2022).
[37]. I. Langmuir, *J. Am. Chem. Soc.* **40**, 1361 (1918).
[38]. E.C. Lima, A. Hosseini-Bandegharaei, I. Anastopoulos, *J. Mol. Liq.* **273**, 425 (2019).
[39]. M.-T. Grandmougin, F. Mayolet, J. Rouet, "*Absorbentes zeolíticos, sus procedimientos de obtención y sus usos para la descarbonatación de flujos gaseosos*", Patent ES2204699T3, 2005.

[40]. R. Hernández Huesca, G. Aguilar Armenta, *J. Mex. Chem. Soc.* **46**, 109 (2002).
[41]. K.A. Babatunde, B.M. Negash, S. Jufar, T.Y. Ahmed, M.R. Mojid, *J. Petrol. Sci. Eng.* **208**, 109466 (2022).
[42]. N. Ayawei, A.N. Ebelegi, D. Wankasi, *J. Chem.* **2017**, 1 (2017).
[43]. R. García Franco, M.A. Hernández, R. Portillo Reyes, V. Petranovskii, E. Rubio, K.F. Quiroz Estrada, *Rev. Int. Contam. Ambient.* **34**, 685 (2018).